Industrial Crops & Products 237 (2025) 122065

Contents lists available at ScienceDirect

Industrial Crops & Products

journal homepage: www.elsevier.com/locate/indcrop

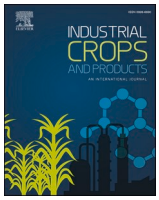

Recycling hemp hurd biowaste into a high-performance cellulose aerogel for oil adsorption and water-in-oil emulsion filtration

Yitong Zhai, Xiaowen Yuan *, Kumar Debajyoti Jena

Future Fibres Laboratory, School of Engineering, Computer and Mathematical Sciences, Auckland University of Technology, Auckland, New Zealand

ARTICLE INFO

Keywords:
Cellulose
Hydrophobic
Aerogel
Hemp hurd
Oil-Water separation

ABSTRACT

A superhydrophobic aerogel derived from hemp hurd, a low-value byproduct of fibre production, is developed for oil-water mixture separation. The fabrication process involves homogenisation, ultrasonication, freeze-drying, and chemical functionalisation using methyltriethoxysilane, yielding a lightweight, porous structure with exceptional hydrophobicity and oleophilicity. Characterisation using scanning electron microscopy confirms a hierarchical micro-nanostructure, while contact angle measurements show a superhydrophobic behaviour (water contact angles $> 150°$). The aerogel exhibits exceptional oil absorption performance, with uptake capacities ranging from 56 to 125 g/g for different oils and organic solvents. It also exhibits excellent mechanical compressibility and reusability, maintaining performance over 50 % of the adsorption capacity after ten adsorption-regeneration cycles. Furthermore, the aerogel also demonstrated excellent performance as a filtration medium for water-in-oil emulsion separations, achieving high flux (665–728 l m^{-2} h^{-1}) and high separation efficiency (97.8–99.1 %). These findings highlight the potential of these hemp hurd-derived aerogels as scalable and environmentally sustainable materials for oil adsorption and water-in-oil emulsion separation.

1. Introduction

Major oil spills, such as the 2010 Deepwater Horizon spill in the Gulf of Mexico and the 2005 Hurricane Katrina-related spill, have caused catastrophic environmental damage, impacting marine ecosystems, wildlife, and coastal communities (Muehlenbachs et al., 2013; Qiao et al., 2025). The large-scale release of crude oil results in persistent contamination of aquatic and terrestrial environments, and substantial economic losses. Various methods have been employed to address water pollution from oil spills, including chemical, biological, and physical approaches. Chemical methods like solidifiers and dispersants are effective but costly (Motta et al., 2018) and can result in secondary pollution (Kleindienst et al., 2015). Biological methods are environmentally friendly but slow and dependent on external factors such as temperature and pH (Fan et al., 2022). Precipitation flotation, while useful, involves extra treatments that add cost and complexity (Wang et al., 2022). Physical sorption, considered more promising, is effective and low-cost, with conventional sorbents like fly ash, synthetic polymers, and natural materials used (Dong et al., 2025; Zamparas et al., 2020). However, they often exhibit low sorption capacity, poor compressive strength, inadequate oil/water selectivity, and have complex fabrication processes (Yu et al., 2021). These shortcomings highlight the need for more effective and efficient sorbent materials.

Aerogels have emerged as a viable alternative due to their lightweight, monolithic structure with 3D interconnected porous structure, which lead to a high specific surface area and exceptional absorption capacity (Fu and Guo, 2022; Ganesamoorthy et al., 2021). In addition, the surface properties of aerogels can be functionalised through various modifications to enhance their ability to selectively adsorb specific types of spills (Gao et al., 2023). Aerogels made from inorganic and petroleum-based materials often suffer from high brittleness and environmental harm, which limit their effectiveness and contributing to ecological damage (Li et al., 2024). In contrast, cellulose-based aerogels have attracted growing attention because of their eco-friendliness, and renewable nature (Zhang et al., 2023). However, cellulose-based aerogels suffer from inherent hydrophilicity, which can hinder their oil adsorption selectivity. To overcome this, surface modification using different types of silanes have been employed in creating superhydrophobic aerogels for selective oil adsorption (Jiang, Zhang, Gao, et al., 2022; Jiang, Zhang, Wang, et al., 2022).

Although previous studies have demonstrated the high efficacy of cellulose-based aerogels for oil adsorption, several challenges remain in

* Corresponding author.
E-mail address: xiaowen.yuan@aut.ac.nz (X. Yuan).

https://doi.org/10.1016/j.indcrop.2025.122065
Received 7 July 2025; Received in revised form 17 September 2025; Accepted 3 October 2025
Available online 25 October 2025

their fabrication. One major concern is the source of raw materials (Lyu et al., 2023). The development of sustainable aerogels necessitates a shift towards utilising cellulose-rich waste materials instead of high-grade cellulosic fibres. Notably, many existing aerogels are synthesised from commercially valuable fibres, which could otherwise be redirected for more economically beneficial applications. As a fast-growing and renewable plant, hemp provides strong, high-aspect-ratio fibres commonly used in textiles, biocomposites, paper, and insulation industries. A large number of cellulose-based materials have been fabricated from hemp. For example, Viscusi et al. prepared organosilane modified hemp fibre as a green sorbent for dye adsorption which shows a high adsorption capacity up to 57.8 mg/g towards methylene blue (Viscusi et al., 2024). Zhu et al. fabricated a superelastic ultralight aerogel assembled from hemp microfibres. The aerogel achieved an high adsorption capacity towards a range of oils and organic solvents (Zhu et al., 2023). The processing of hemp fibres generates significant plant waste, including noil, stems, and hurd, which are traditionally considered worthless. Repurposing these waste products not only provides a sustainable source of cellulose but also addresses agricultural waste management by converting waste materials into high value-added products (Kaur et al., 2023; Paulauskiene et al., 2023; Wang et al., 2024).

Hemp hurd, the woody core of the hemp stalk, is a lignocellulosic material primarily composed of cellulose (40–48 %), hemicellulose (18–24 %), and lignin (21–24 %), along with minor amounts of extractives (2–5 %), ash (1–3 %), and moisture (Gümüşkaya et al., 2007). Physically, it is lightweight, with a bulk density typically ranging from 88 to 133 kg/m^3 (Fehrmann et al., 2023), and exhibits a porous, fibrous structure that offers high absorbency and good thermal and acoustic insulation properties. The cellulose provides structural strength, hemicellulose adds flexibility, and lignin contributes to rigidity and resistance to microbial degradation. Despite their abundance, hemp hurds are commonly regarded as agricultural waste and are typically discarded following the extraction of hemp bast fibres. Valorising this underutilised biomass for the fabrication of cellulose-based aerogels not only mitigates processing waste but also offers a sustainable alternative to conventional materials, thereby fostering environmentally friendly practices and promoting efficient resource utilisation.

In this study, we present a simple approach for the preparation of superhydrophobic cellulose aerogels for oil adsorption and emulsion separation from hemp hurd. The extraction of cellulose from hemp hurd was achieved through a bleaching process using $NaClO_2$, followed by alkaline treatment with NaOH. These cellulose fibres were subsequently processed into a suspension of cellulose microfibres (CMF) through homogenisation and ultrasonic treatment. Ultra-lightweight hemp aerogels were subsequently assembled from the aqueous CMF suspension via lyophilisation. Hydrophobic properties were imparted to the aerogels through chemical vapour deposition using MTES. The resulting aerogels exhibited superhydrophobicity with high oil absorption capacities. The use of cost-effectiveness, readily available raw materials and chemicals enables scalable production, positioning hemp hurd-based aerogels as a viable alternative with potential for diverse applications.

2. Materials and methods

2.1. Materials

The raw hemp hurd (RHH) bio-waste was obtained from Hemp New Zealand after the bast fibre extraction. Sodium hydroxide (NaOH, AR) and absolute ethyl alcohol (C_2H_5OH) were purchased from Thermo Fisher Scientific. Sodium chlorite ($NaClO_2$, 80 %) and methyltriethoxysilane (MTES, 99 %) were sourced from Sigma-Aldrich. The crosslinker, 1,2-bis(triethoxysilyl)ethane (BTESE, 95 %), was acquired from Shanghai Macklin Biochemical Technology Co., Ltd. Deionized (DI) water, supplied by School of Science at Auckland University of Technology, was utilised for all synthesis procedures.

2.2. Extraction of cellulose

The wax and other impurities from RHH were removed by boiling it in DI water for 2 h. Following washing, the RHH was oven-dried at 80°C for 12 h. The dry RHH was then crushed using a commercial grinder and sieved through a mesh to obtain uniform sized RHH powder. The washed RHH was then bleached in 1.4 wt% $NaClO_2$ solution, with the pH adjusted to 3–4 using CH_3COOH, and heated at 70°C for 2 h. The bleached hemp hurd (BHH) was then subjected to an alkali treatment in 4 wt% NaOH solution. The alkali-treated fibres were washed to neutral by rinsing three times with DI water and then dried at 70°C overnight. The extracted cellulose fibres (CF) were stored as a suspension in DI water at 4°C in a fridge or freeze-dried.

2.3. Fabrication of superhydrophobic aerogel

Fig. 1 shows the fabrication process of superhydrophobic aerogel from the cellulose extracted from RHH. A 0.5 wt% suspension was prepared and homogenised in a high-speed shearing homogeniser, followed by ultrasonication to obtain a cellulose microfibre (CMF) suspension. BTESE was then added dropwise into the suspension and kept stirring for 30 min. The suspension was pre-frozen using liquid nitrogen (-198°C) and freeze-dried at −78°C to make ultra-lightweight aerogels (HA). The freeze-dried aerogel was then placed in an oven at 80°C for 12 h to facilitate the crosslinking. The hydrophobisation of the aerogels (HHA) was performed by exposing them to MTES in a desiccator, with the MTES coating achieved through chemical vapour deposition (CVD).

2.4. Characterisations

The apparent density of the aerogels is determined by the ratio of their mass (m) to their apparent volume (V) using the formula:

$$\rho = \frac{m}{V}$$

where ρ represents the density of the aerogel(g/cm^3), m represents the weight of the aerogel (g), and V is the apparent volume (cm^3).

Porosity (P) is determined using the following equation:

$$P = \left(1 - \frac{\rho}{\rho s}\right) \times 100$$

where: P is the porosity expressed as a percentage, ρ is the apparent density of the aerogel (g/cm^3), and ρ_s is the density of the solid skeleton of the aerogel (1.5 g/cm^3) (Zhai et al., 2023).

The surface morphology of RHH, BHH, CF, HA, and HHA were examined using a Hitachi SU-70 Schottky field emission scanning electron microscope (FESEM). Elemental analysis was performed via energy dispersive spectroscopy (EDS) utilising a Thermo Scientific NORAN System 7 (NSS) version 3.3.113. The thermal stability and decomposition behaviour of HA and HHA were evaluated using a Thermogravimetric analyser (Q5000, TA Instruments, U.S.A) under a nitrogen atmosphere (25 ml/min) with the temperature ramped from 25 to 700℃ at a heating rate of 10℃/min. Fourier-transform infrared (FTIR) spectra were recorded in transmission mode using a PerkinElmer FTIR Spectrometer across a wavelength range of 550–4000 cm^{-1}. The crystal structure of the prepared samples was characterised by X-ray diffraction (XRD) using a Rigaku Ultima IV X-ray diffractometer with Cu Kα radiation (λ = 0.15418 nm) at 40 kV and 20 mA. XRD measurements were conducted at a scanning rate of 5°/min within a diffraction angular (2θ) range of 10° to 60°. The water contact angle of the HA and HHA was measured using an Ossila contact angle goniometer. The mechanical properties of the aerogel were determined through compression testing using an Instron 5848 system, equipped with a 100 N load cell at a

Fig. 1. The fabrication process of the hemp aerogels (HA and HHA).

constant compression rate of 5 mm/min.

2.5. Oil-in-water emulsion separation

The water-in-oil emulsions were prepared by dispersing 1 ml of deionised water into 99 ml of the selected oil, followed by high-speed blending using an IKA T25 digital ULTRA-TURRAX blender at 8000 rpm for 20 min to obtain the stable emulsion. Optical microscopy was employed to investigate the prepared emulsion and the filtrate. HHR was inserted into the bottom of a 20 ml syringe to form the filtration apparatus. The emulsions were then poured into the syringe to start the filtration process. The flux ($l\ m^{-2}h^{-1}$) was calculated according to the following equation

$$Flux = \frac{V}{A \times t}$$

where V denotes the volume of the emulsion that passed through the system, A and t are the cross-section area of the syringe and time, respectively.

A Karl Fischer titrator was employed to determine the water concentration in the filtrate, and the separation efficiency (E) was determined by:

$$E = \frac{C_0 - C_1}{C_0} \times 100\%$$

C_0 and C_1 are the water concentration of the emulsion and filtrate,

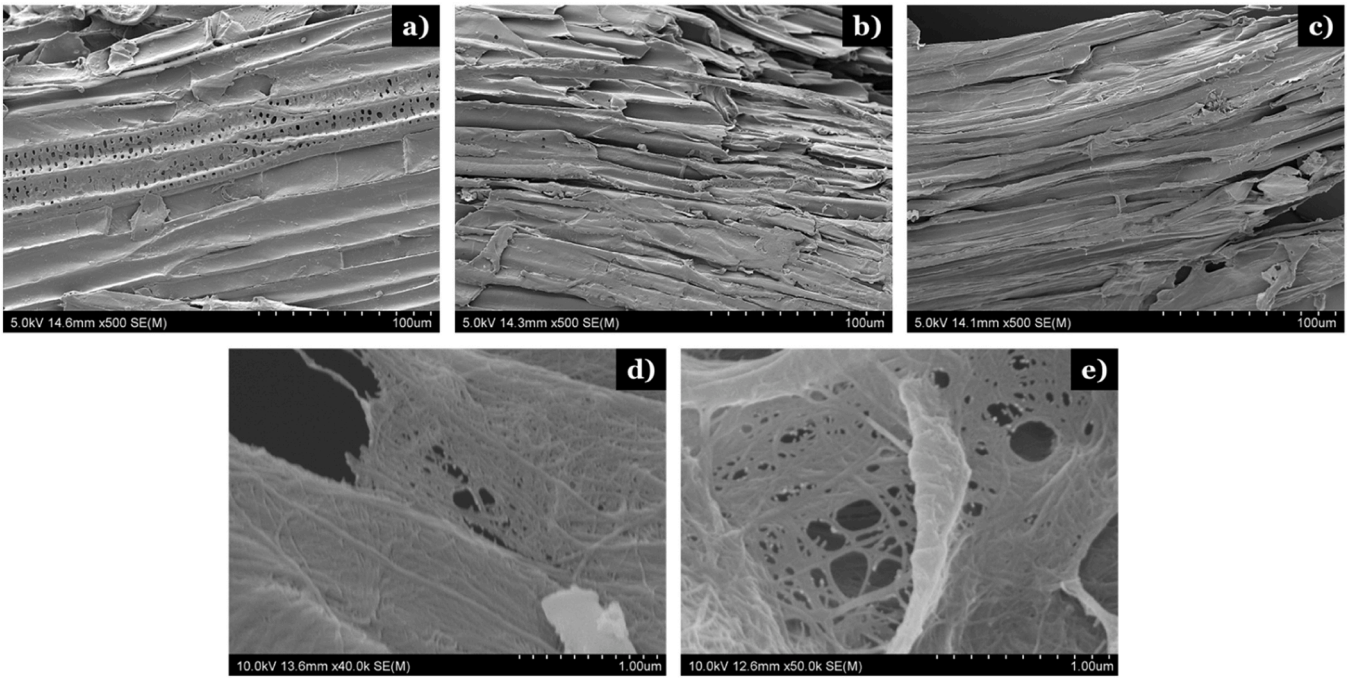

Fig. 2. SEM images of (a) RHH; (b) BHH; (c) CF; (d) HA; and (e) HHA.

respectively.

3. Results and discussion

3.1. Structural and chemical characterisation of the hemp aerogel

The changes in surface morphology of the RHH after bleaching (BHH) and alkali treatment (CF) is shown in Fig. 2a-c. The surface morphology of hemp hurd undergoes significant changes following the bleaching and alkali treatments, which are primarily aimed at removing lignin and hemicellulose, respectively. During the bleaching process, lignin, a complex polymer that binds cellulose fibres together and gives the hemp hurd its rigidity and colour is removed. As lignin is extracted, the surface of the BHH becomes more fibrous. The previously compact and rigid structure loosens, revealing the underlying cellulose fibres. This process also results in a lighter colour and a rougher surface texture, as the removal of lignin exposes more of the cellulose matrix. The subsequent alkali treatment targets the removal of hemicellulose, a polysaccharide that surrounds the cellulose fibres and contributes to the structural integrity of the plant cell walls. As hemicellulose is removed, the surface morphology of CF (Fig. 2c) possesses a collapsed structure. The alkali treatment typically results in the swelling and partial disintegration of the fibre structure, leading to an even more fibrillated surface and the fibres collapsed onto itself. The cellulose fibres become more distinct and are less embedded within the matrix, as the supporting hemicellulose is stripped away. This treatment increases the accessibility of the CF for further processing, leaving behind a more purified cellulose-rich structure with enhanced surface area and reactivity. The SEM images of the hemp aerogel before and after MTES treatment (Fig. 2d-e) reveal a highly porous, three-dimensional interconnected network. The fibres appear thin and elongated, forming a delicate web-like matrix with substantial voids between them. This structure underscores the effectiveness of the homogenisation and freeze-drying processes in producing a lightweight and highly porous material. The apparent density and porosity of the HA aerogel is determined to be 8 mg/cm^3 and 99.5 %, respectively. The open, porous network is indicative of the aerogel's low density. The rough surface of the fibres, coupled with their intricate, interconnected arrangement, suggests a high surface area, enhancing the aerogel's suitability for oil adsorption applications.

The EDS mapping presented in Fig. 3a-b offers a comparative analysis of the elemental distribution within the hemp aerogel before and after the application of the MTES coating. The EDS map of the uncoated, control aerogel (Fig. 3a) predominantly displays the presence of carbon (C) and oxygen (O), which is expected given the cellulose-based composition of the aerogel. The absence of other elements reinforces the conclusion that the aerogel is composed almost entirely of cellulose with minimal impurities. In contrast, the EDS map of the MTES-coated aerogel (Fig. 3b) reveals the presence of silicon (Si), which is absent in the control sample. The detection of Si indicates that MTES has been successfully deposited onto the aerogel's surface, forming a silane layer that imparts hydrophobic properties to the aerogel. The presence of Si alongside the persistent peaks of C and O suggests that the fundamental cellulose structure remains intact while the chemical modification introduces the desired hydrophobic characteristics.

Fig. 4a illustrates the FTIR spectra of RHH, BHH, and CF, showcasing the chemical transformations that occur during each processing step. The FTIR spectrum of RHH displays distinct absorption bands at approximately 3330 cm^{-1} , corresponding to O-H stretching (Viscusi et al., 2020); 2900 cm^{-1} , indicative of C-H stretching; and 1733 cm^{-1} , associated with the C═O stretching vibration attributed to the acetyl group in hemicellulose or ester linkage present in lignin (Bokhari et al., 2021). The presence of lignin is evident from the peaks at 1505 cm^{-1} , 1596 cm^{-1} , and 1462 cm^{-1} , which correspond to aromatic vibrations and C-H stretching. The band at 1239 cm^{-1} is ascribed to C-O-C stretching of the aryl-alkyl ether linkage in hemicellulose, while the 1030 cm^{-1} band represents C-O stretching vibrations in cellulose. Additionally, the band at 900 cm^{-1} is associated with the glycosidic bond in cellulose (Stevulova et al., 2014). Following the bleaching process, the FTIR spectrum of BHH shows a marked reduction in the peak at 1733 cm^{-1} , indicating removal of hemicellulose and lignin. The disappearance of the lignin-related peaks at 1505 cm^{-1} further confirms the complete removal of lignin after bleaching (Zhai et al., 2023). However, the O-H, C-O, and C-H stretching bands corresponding to cellulose remain present, reflecting the retention of cellulose. In the spectrum of CF, the absence of peaks at 1733 cm^{-1} and 1239 cm^{-1} indicates the complete removal of hemicellulose. The disappearance of lignin and hemicellulose-associated peaks confirms that the chemical treatment has effectively isolated cellulose by eliminating the non-cellulosic components. Fig. 4b presents the FTIR spectra of the control hemp aerogel (HA) and the MTES-coated hemp aerogel (HHA). The spectrum of HA displays characteristic cellulose peaks, including a

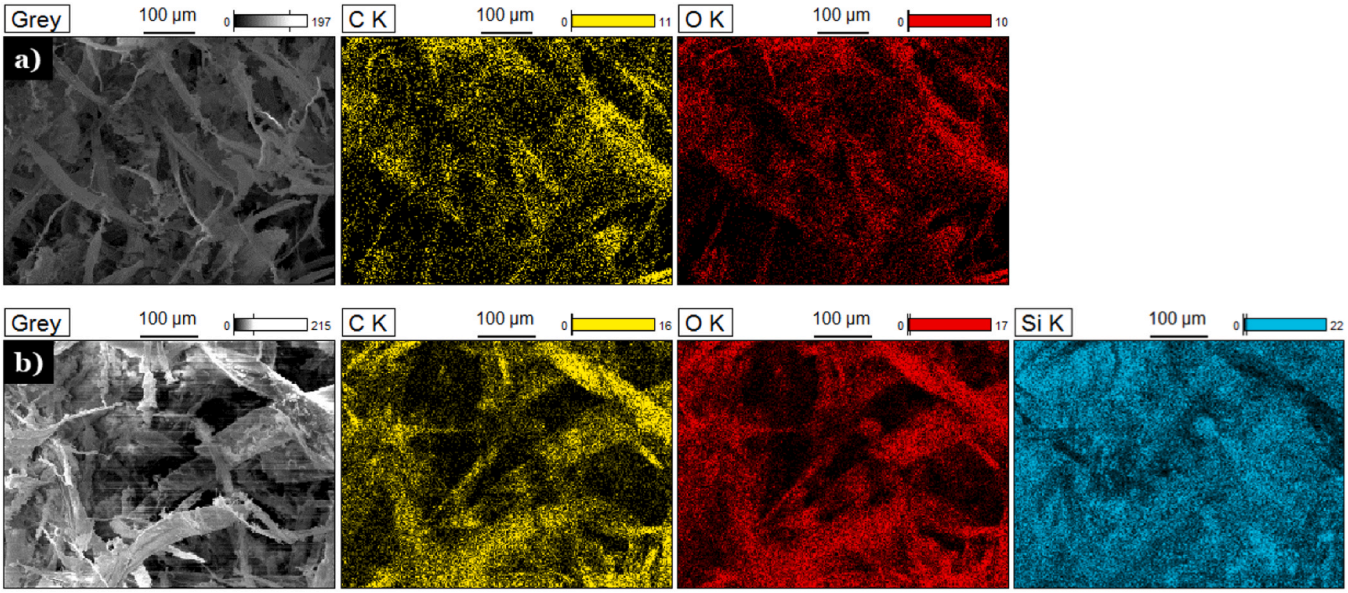

Fig. 3. EDS map of (a) HA and (b) HHA.

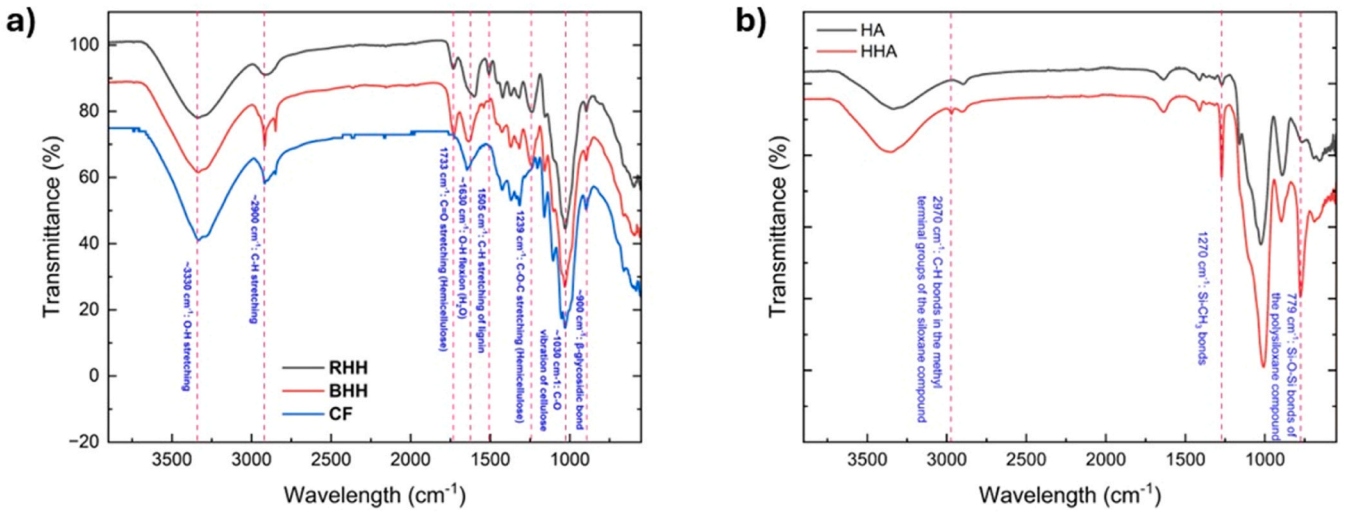

Fig. 4. FTIR spectra of (a) RHH, BHH, and CF; (b) HA and HHA aerogel.

broad O-H stretching band around 3330 cm^{-1} , a C-H stretching band around 2900 cm^{-1} , and C-O stretching vibrations between 1030 and 1230 cm^{-1} . Upon coating with MTES, the FTIR spectrum of the HHA aerogel reveals the emergence of new peaks at approximately 1270 cm^{-1} and 779 cm^{-1} , corresponding to Si-CH_3 and Si-O-Si stretching vibrations, respectively. Additionally, a small peak appears at 2970 cm^{-1} , which is attributed to the C-H bonds in the methyl terminal groups of the siloxane compound. These newly formed peaks confirm the successful attachment of silane groups to the aerogel surface, indicating the formation of a silane layer.

Fig. S1 shows the XRD spectra of HA aerogel and silane-modified HHA aerogel. The diffraction peaks observed for HA aerogel at $2\theta = 14.6°$ and 22.8° correspond to the (110) and (200) planes, characteristic of the cellulose type I structure. Similarly, the XRD spectra of silane-modified HHA aerogel also display peaks at the same 2θ values, indicating that the silane modification primarily affects the hydroxyl groups on the surface of the CNF aerogels without altering the cellulose I structure (M et al., 2019). The thermogravimetric analysis (TGA) results of HA and HHA reveal their thermal decomposition behaviour and stability. As shown in Fig. S2, the initial weight loss observed below 160°C is attributed to the evaporation of adsorbed moisture and other volatile compounds. HHA demonstrates a lower weight loss at this region. This is due to the more hydrophilic nature of HA aerogel which can absorb more moisture from the air compared with a hydrophobic HHA aerogel. The primary decomposition occurs between 160°C and 400°C, corresponding to the thermal degradation of cellulose. HHA demonstrates higher thermal stability than HA, as evidenced by its marginally higher residual weight above 400°C, likely due to the protective effect of the silane coating. The derivative thermogravimetric (DTG) curves further show maximum degradation temperatures at ~351°C for HHA and ~346°C for HA, indicating a slight enhancement in thermal stability for HHA. This shift suggests that the hydrophobic silane layer delays the decomposition of the aerogel matrix. These findings confirm that the hydrophobisation process not only improves the hydrophobicity of the aerogel but also enhances its thermal resistance.

The mechanical properties of aerogel are critical for its application in oil adsorption. The mechanical properties of HHA were characterised using a compression test, and the corresponding stress-strain curve is shown in Fig. 5. Two distinct regions were observed, namely, an initial elastic region (strain < ~50 %) where the stress increased linearly with the increased strain; and a densification region (strain > ~50 %), where the stress increased significantly with the increased strain. Similar compression behaviour is observed in other reported cellulose-based aerogels (Zhou et al., 2016). The first region is ascribed to the elastic

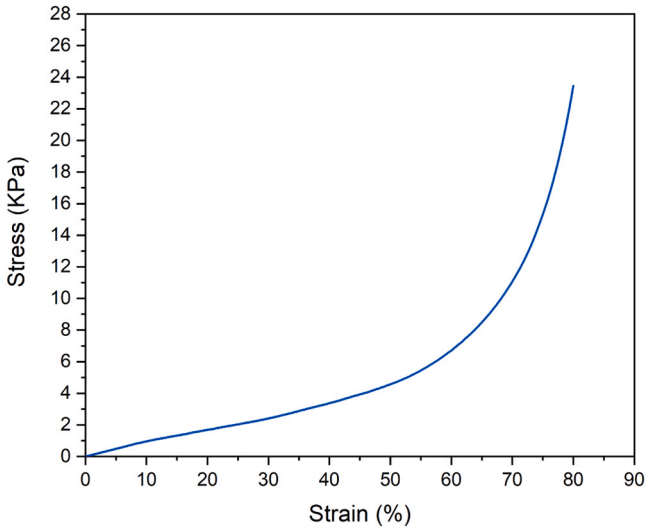

Fig. 5. Compression test results for HHA.

deformation of the continuous aerogel fibre skeleton, and the gradual deformation of the pores. In the following densification region, as strain continuously increases, the pores are severely deformed, and the pore walls begin to contact each other resulting in the formation of dense load-bearing structures. Therefore, the stress exhibited a sharp rise with the increased strain (Sadat Fazel et al., 2024).

3.2. *Hydrophobicity of the hemp aerogel*

The control aerogel (HA) exhibits rapid water absorption, likely due to the abundant hydroxyl groups present in the cellulose structure. The incorporation of surface silane groups via the MTES coating imparts a hydrophobic layer on the HHA aerogel. Fig. 6a demonstrates the enhanced water repellency of the HHA aerogel compared with the control, as it repels water droplets and floats on the water surface without any visible absorption. The HHA aerogel also exhibits excellent oleophilicity, as vegetable oil and other organic solvents are completely adsorbed, with the red-stained regions (vegetable oil dyed with Sudan III) visibly marking absorption. The superhydrophobicity of the modified aerogel is further confirmed by the water contact angle measurements shown in Fig. 6b, where the contact angle exceeds 150°, indicating extreme resistance to water adhesion. The MTES coating

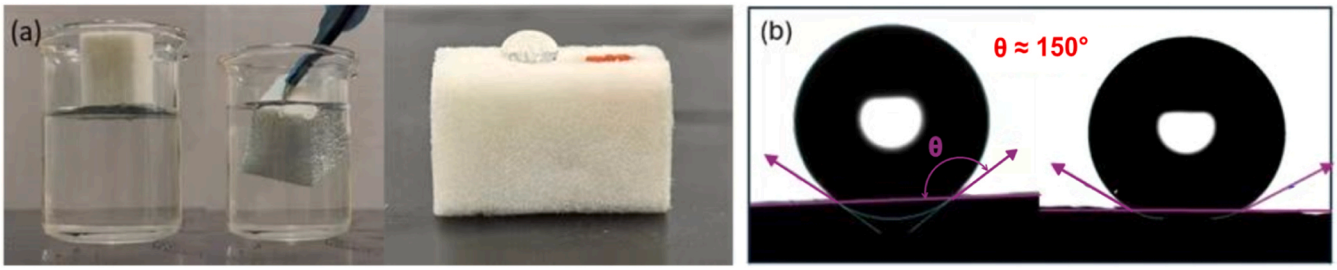

Fig. 6. (a) Demonstration of water repellency and oleophilicity of the HHA aerogel. The aerogel repels water, floating on the surface without absorption, and readily absorbs vegetable oil stained with Sudan III. (b) Water contact angle measurement of the HHA aerogel, showing a contact angle exceeding 150°, confirming its superhydrophobic nature.

significantly enhances hydrophobicity by introducing silane groups that lower the surface energy and causes water droplets to bead up rather than spread out on the aerogel surface. These findings confirm the silane-functionalised hemp aerogel's high hydrophobicity and oleophilicity, making it a promising candidate for oil-water separation and environmental remediation applications.

3.3. Oil adsorption capacity

Due to its excellent hydrophobicity, the HHA aerogel showed a good oil adsorption selectivity from an oil/water mixture. Fig. 7a shows the selective vegetable oil adsorption process of HHA from a simulated oil/water mixture. The aerogel floated on the water surface and quickly absorbed the floating oil upon contacted with the oil contaminates. The adsorption process is completed in less than a minute. After oil adsorption is complete, the aerogel still floated on the surface of water, demonstrating its high hydrophobicity and ultralow density. Additionally, Fig. 7b shows that the prepared aerogel could also be used to absorb dichloromethane (dyed with Sudan III) from under the water.

To further evaluate the oil adsorption performance of the synthesised HHA, a range of oils and organic solvents including chloroform, dimethylformamide, dichloromethane, toluene, hexane, acetone, vegetable oil, and silicone oil were employed to assess its superior adsorption capacity. The adsorption capacity (g/g) is defined as the weight of the adsorbed oil (g) to the dry weight of the HHA sample (g). As shown in Fig. 8a and b, the HHA aerogel exhibited an exceptional adsorption capacity ranging from 56 to 125 g/g, with a range of oils and organic solvents. The adsorption process of HHA for those non-polar oily contaminates can be divided into three steps: (1) Initial diffusion of the liquid onto the aerogel surface and into its porous network, (2) Pore filling accompanied by capillary retention of the organic liquids, and (3) Accumulation and storage of the adsorbed liquid within the internal porous structure of the aerogel. Overall, the adsorption capacity of HHA fabricated in this study is comparable to several previously reported cellulose-based aerogels, such as the cotton-cellulose aerogel modified with methyltrimethoxysilane through CVD (up to 100 g/g) (Cheng et al., 2017), kapok/microfibrillated cellulose aerogels treated with vinyltrimethoxysilane (130 g/g) (Zhang et al., 2021), and methyltrimethoxysilane coated recycled cellulose aerogels (up to 95 g/g) (Feng et al., 2015). Interestingly, the oil adsorption performance of HHA is better than some cellulose-based aerogels which underwent more sophisticated treatment, such as the styrene/acrylic monomers modified cellulose nanofibre aerogel (30 g/g) (Mulyadi et al., 2016). Moreover, compared with the synthetic polymer-based oil sorbents, the HHA showed much higher adsorption capacities, including activated carbon enhanced thermoplastic polyurethane composite aerogel (up to 39.6 g/g) (Wang et al., 2023), melamine formaldehyde composite foam (12 – 25 g/g) (Jin et al., 2022), and poly (vinylidene fluoride) aerogel (3 – 7 g/g) (Chen et al., 2017). Although the adsorption capacities of HHA were comparatively lower than those of graphene- and carbon

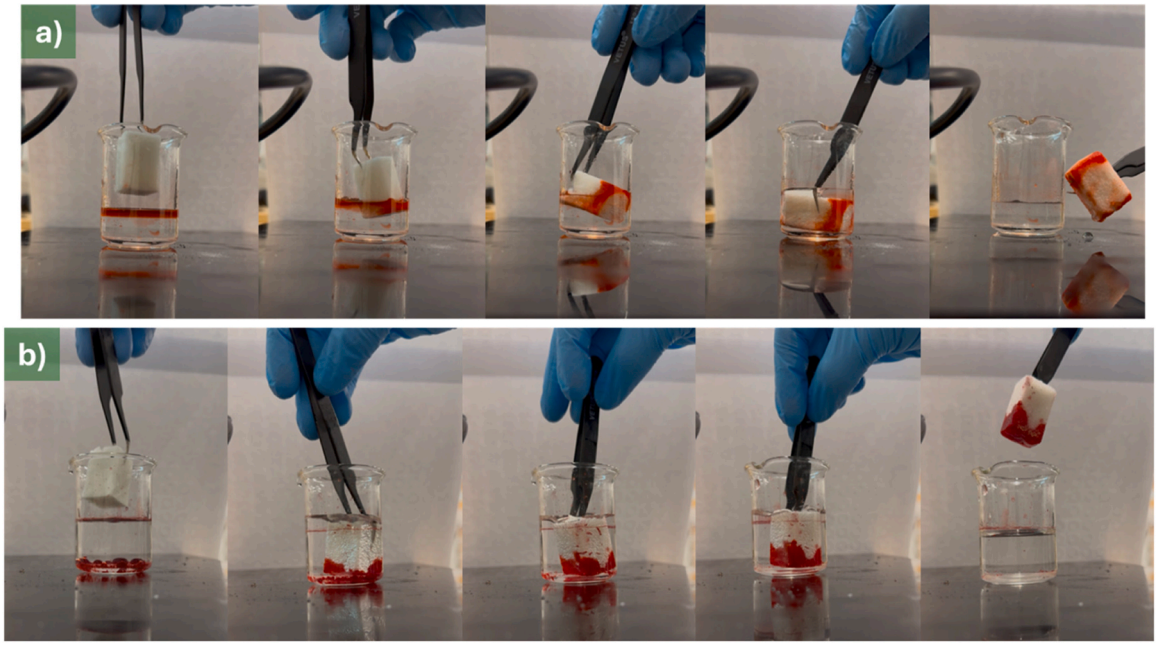

Fig. 7. (a) Vegetable oil adsorption from the water surface using HHA. (b) Dichloromethane adsorption from under the water using HHA.

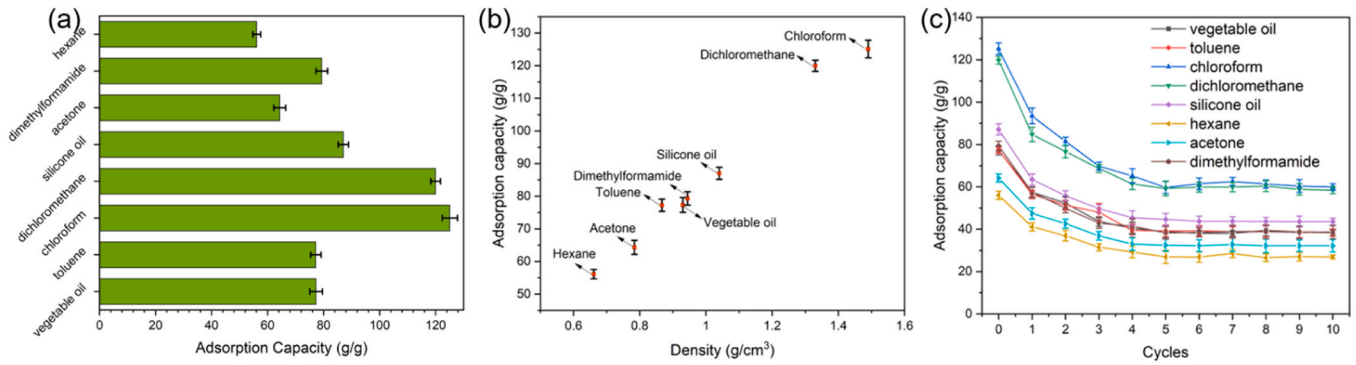

Fig. 8. (a) Adsorption capacity of HHA with a variety of oils and organic solvents. (b) Adsorption capacity of HHA as a function of the density of the oils and organic solvents. (c) Adsorption capacity of HHA after each adsorption-release cycle.

nanotube-based aerogels, its low cost and minimal chemical processing requirements make it a promising candidate for the selective removal of oily contaminants from oil/water mixtures.

The reusability of HHA for oil adsorption was characterised by cyclic adsorption testing. The HHA was first dipped into the oil to reach adsorption saturation, which was then compressed using two glass slides to release the adsorbed oil and resubmerged into the oil for the next adsorption. The adsorption capacity values were recorded after each cycle. As shown in Fig. 8c, a significant reduction of adsorption capacity was observed after the first adsorption-compression cycle. The adsorption capacity of HHA for vegetable oils in the second adsorption test reduced from 77.3 g to 57.2 g, which was approximately 75 % of its initial value. Similar reduction trends were also observed for all the remaining tested oils. This was attributed to the irreversible structural damage to the aerogel samples caused by mechanical compression. However, the adsorption capacities of HHA stabilised at about 50 % of their initial values after five cycles, which indicates its good compressibility and reusability.

3.4. Oil adsorption kinetics

To further investigate the adsorption kinetics of HHA, vegetable oil and hexane were selected as representative adsorbates for data collection. The experimental adsorption data were fitted using the pseudo-first order (Eq. (1)) and pseudo-second order (Eq. (2)) kinetic models.

$$\ln(q_e - q_t) = \ln q_e - k_1 t \tag{1}$$

$$q_t = \frac{k_2 q_e^2 t}{1 + k_2 q_e t} \tag{2}$$

where q_e (g/g) and q_t (g/g) represent the adsorption capacity at equilibrium and at time t, respectively; t (s) denotes the adsorption time; and k_1 and k_2 are the rate constants of the pseudo-first-order and pseudo-second-order models, respectively.

The correlation between the fitting model and the experimental data was evaluated by comparing the correlation coefficient (R^2) and calculating the value of root-mean-square-deviation (RMSD), which is defined by Eq. (3) as follows:

$$\mathrm{RMSD} = \sqrt{\frac{\sum(q_{t(\mathrm{exp})} - q_{t(\mathrm{fit})})}{N}} \tag{10}$$

where N is the number of experimental data points ($N = 13$), $q_{t(\mathrm{exp})}$ (g/g) denotes the experimental adsorption capacity data at time t, and $q_{t(\mathrm{fit})}$ (g/g) represents the corresponding adsorption capacity predicted by the fitted kinetic model.

Fig. 9 shows the fitted curves of the experimental data using the two kinetic models, and the corresponding parameters are summarised in Table 1. As shown in the figure, the q_t – t curve indicated the oil adsorption process of HHA is fast in the initial step followed by a levelling off. This is because there is more available pore space to adsorb the oil at the initial stage, however, as adsorption progresses, less space is available for oil to occupy. Comparing the two models, the pseudo-first-order model showed a higher R^2 value and lower RMSD values in both vegetable oil and hexanes, which indicate a better suitability to

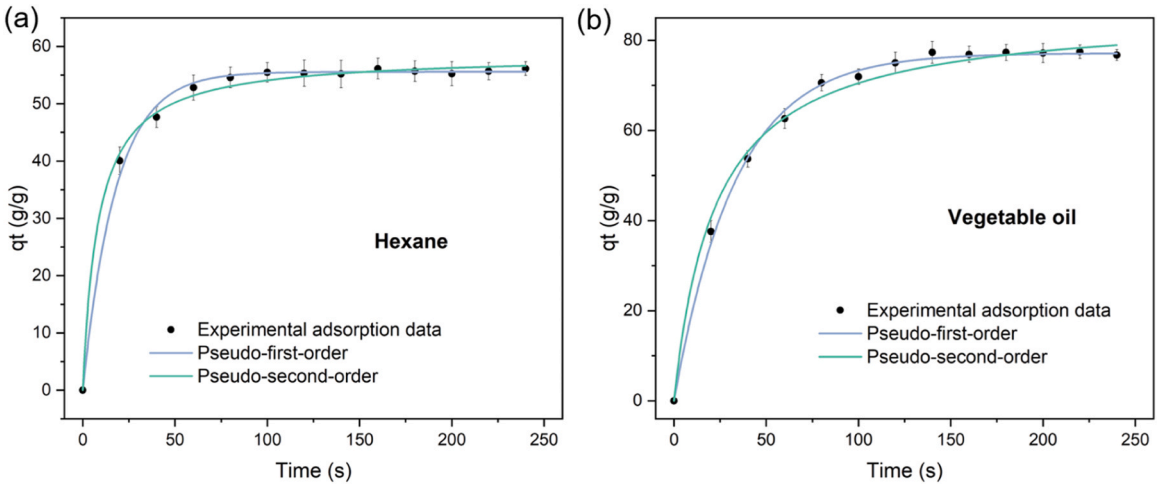

Fig. 9. Adsorption kinetics of HHA for (a) vegetable oil and (b) hexane.

Table 1
Kinetic parameters of the pseudo-first order and pseudo-second order models used to fit the experimental oil adsorption data.

Oils	Pseudo-first order				Pseudo-second order			
	k_1	q_e	R^2	RMSD	k_2	q_e	R^2	RMSD
Vegetable oil	0.0303	77.17	0.998	1.09	0.00047	87.90	0.982	1.77
Hexane	0.059	55.37	0.996	0.94	0.0016	59.80	0.962	16.72

describe the adsorption process of HHA. Moreover, the calculated q_e values in the pseudo-first-order model are closer to the experimental data.

3.5. Water-in-oil emulsion separation

Unlike the simple oil/water mixtures, emulsions represent a more complex scenario which cannot be separated through a conventional adsorption approach. Identifying low-cost and efficient methods for their separation remains a major challenge in the field. To further characterise the water/oil emulsion separation performance of the HHR, a solely gravity-driven separation process was established as shown in Fig. 10a. HHR was placed in the bottom of a syringe acting as a thick filer and the prepared water-in-oil emulsion was poured into the setup to start the separation. Three different water-in-oil emulsions were tested, including water-in-vegetable oil, water-in-toluene, and water-in-silicon oil. The milky emulsion was continuously filtered by the HHR and the filtrate appeared transparent, demonstrating the successful separation of the milky emulsion. Optical microscope images further showed the successful separation. Before filtration, water droplets with diameter between 1 and 9 μm were observed in the freshly prepared emulsion (Fig. 10b), whereas no droplets were found in the filtrate (Fig. 10c). The separation efficiency of this gravity-driven setup towards the above three emulsions were between 97.8 % and 99.1 % and the flux between 665 and 728 l m^{-2} h^{-1}.

The high separation efficiency and high flux of RHH is attributed to its unique coalescence and size-sieving separation mechanisms (Li et al., 2019). The process involves two sequential steps: demulsification followed by phase separation. Upon contact with the aerogel's hierarchically porous structure, the water-in-oil emulsions experience enhanced interaction with the aerogel surface. The strong intermolecular forces between the superhydrophobic aerogel and the hydrophobic surface of the dispersed droplets facilitate the demulsification process. The combination of hierarchical porosity and superhydrophobicity enables a high demulsification efficiency. Subsequently, the continuous oil phase permeated through the aerogel filter and drained into the bottom beaker, while the separated water droplets were blocked and coalesced into larger aggregates within the tortuous microchannels and are retained by the aerogel filter. In contrast, conventional membranes separate the emulsions mainly via size-sieving mechanisms, which relies on the high density of micropores. These membranes typically require external pressure to overcome resistance and achieve separation, as gravity alone is insufficient due to the small pore dimensions. Furthermore, their limited pore volume and short permeation paths lead to rapid performance degradation, often caused by surfactant adsorption and pore blockage, resulting in a significant decline in flux. Compared to such membranes, the HHR developed in this study offers distinct advantages, including high porosity and extended permeation channels, which contribute to its prolonged operational lifetimes without significant pore fouling. The synergy of high demulsification efficiency and porosity enables aerogels to deliver high separation fluxes and high separation efficiencies.

4. Conclusion

An ultra-lightweight and superhydrophobic aerogel suitable for oil adsorption and water-in-oil emulsion separation were successfully derived from bio-waste hemp hurd. Cellulose was first extracted from raw hemp hurd through sequential sodium chlorite bleaching and alkali treatment. Superhydrophobic cellulose-based aerogel was then

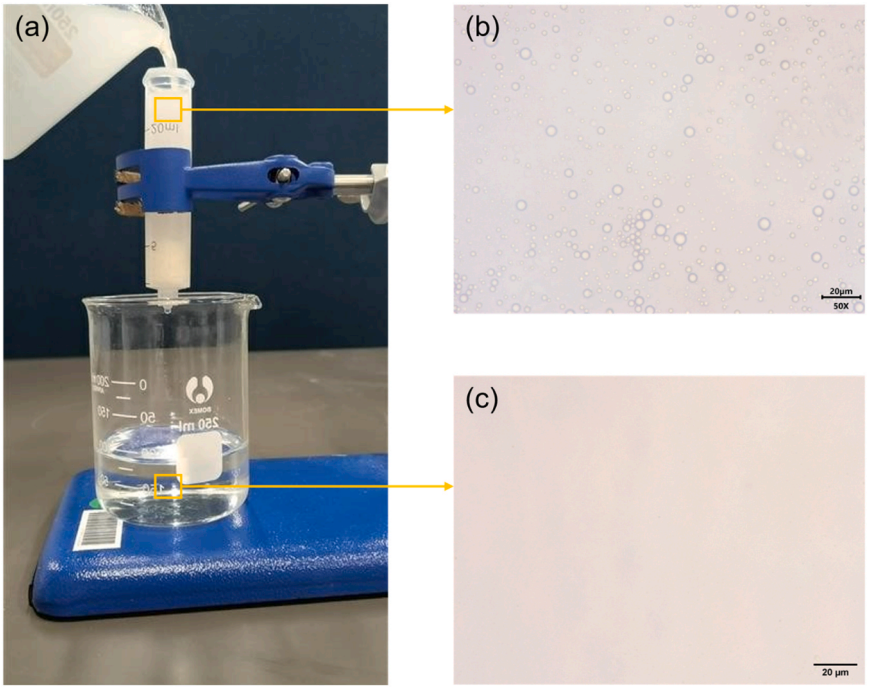

Fig. 10. (a) Filtration apparatus for the water-in-oil emulsion. (b) Optical microscope image of the feed emulsion. (c) Optical microscope image of the filtrate.

fabricated via freeze-drying and modified with MTES through CVD. The entire process is cost-effective and straightforward in comparison with other hemp fibre derived oil sorbents which start with high-cost hemp fibres as raw materials and involve a complicated supercritical CO_2 drying method for aerogel preparation. FTIR results confirmed the effective removal of non-cellulosic components from the raw materials. SEM analysis revealed a hierarchical micro-nanostructure and a porous architecture, enhancing the aerogel's suitability for oil absorption applications. Additionally, TGA indicated high thermal stability, with HHA exhibiting a maximum degradation temperature of ~351 °C, slightly higher than the control aerogel HA. The introduction of silane functional groups via MTES treatment was validated with a significant increase in the water contact angle (>150°), confirming excellent superhydrophobic behaviour. Performance evaluation highlighted the aerogel's outstanding oil adsorption capacities. Despite an initial reduction in adsorption capacity during cyclic tests, the aerogel stabilised at approximately 50 % of its original capacity after five cycles, demonstrating good compressibility and reusability. Moreover, the aerogel could be used as a filter to separate water-in-oil emulsions with a high separation efficiency and high flux. Although promising results have been shown, the gaseous phase CVD method utilised here may result in the inhomogeneous modification of the aerogel outer and inner surface. This might affect the long-term performance of the aerogel. A more homogeneous modification method is needed for future research.

CRediT authorship contribution statement

Xiaowen Yuan: Writing – review & editing, Supervision, Resources, Project administration, Conceptualization, Funding acquisition, Methodology. **Kumar Debajyoti Jena:** Writing – original draft, Methodology, Formal analysis, Conceptualization, Investigation, Validation. **Yitong Zhai:** Writing – review & editing, Writing – original draft, Formal analysis, Investigation.

Declaration of Competing Interest

The authors declare that they have no known competing financial interests or personal relationships that could have appeared to influence the work reported in this paper.

Acknowledgements

The authors acknowledge Hemp New Zealand Ltd for providing hemp hurd and supporting this project.

Appendix A. Supporting information

Supplementary data associated with this article can be found in the online version at doi:10.1016/j.indcrop.2025.122065.

Data availability

Data will be made available on request.

References

Bokhari, S.M., Chi, K., Catchmark, J.M., 2021. Structural and physico-chemical characterization of industrial hemp hurd: impacts of chemical pretreatments and mechanical refining. Ind. Crops Prod. 171, 113818. https://doi.org/10.1016/j.indcrop.2021.113818.

Chen, X., Liang, Y.N., Tang, X.-Z., Shen, W., Hu, X., 2017. Additive-free poly (vinylidene fluoride) aerogel for oil/water separation and rapid oil absorption. Chem. Eng. J. 308, 18–26.

Cheng, H., Gu, B., Pennefather, M.P., Nguyen, T.X., Phan-Thien, N., Duong, H.M., 2017. Cotton aerogels and cotton-cellulose aerogels from environmental waste for oil spillage cleanup. Mater. Des. 130, 452–458.

Dong, S., Li, Y., Zhu, K., Wang, C., Zhai, S., 2025. Advances in structure designing and function tailoring strategy toward alginate-based hydrogels for efficient water remediation: a review, 2025/04/01/ Int. J. Biol. Macromol. 304, 140801. https://doi.org/10.1016/j.ijbiomac.2025.140801.

Fan, Q., Lu, T., Deng, Y., Zhang, Y., Ma, W., Xiong, R., Huang, C., 2022. Bio-based materials with special wettability for oil-water separation, 2022/09/15/ Sep. Purif. Technol. 297, 121445. https://doi.org/10.1016/j.seppur.2022.121445.

Fehrmann, J., Belleville, B., Ozarska, B., Gutowski, W.S., Wilson, D., 2023. Influence of particle granulometry and panel composition on the physico-mechanical properties of ultra-low-density hemp hurd particleboard. Polym. Compos. 44 (11), 7363–7383. https://doi.org/10.1002/pc.27631.

Feng, J., Nguyen, S.T., Fan, Z., Duong, H.M., 2015. Advanced fabrication and oil absorption properties of super-hydrophobic recycled cellulose aerogels. Chem. Eng. J. 270, 168–175.

Fu, Y., Guo, Z., 2022. Natural polysaccharide-based aerogels and their applications in oil–water separations: a review [10.1039/D2TA00708H]. J. Mater. Chem. A 10 (15), 8129–8158. https://doi.org/10.1039/D2TA00708H.

Ganesamoorthy, R., Vadivel, V.K., Kumar, R., Kushwaha, O.S., Mamane, H., 2021. Aerogels for water treatment: a review, 2021/12/20/ J. Clean. Prod. 329, 129713. https://doi.org/10.1016/j.jclepro.2021.129713.

Gao, J., Wang, J., Cai, M., Xu, Q., Zhang, J., Cao, X., Zhang, J., Chen, Y., 2023. Advanced superhydrophobic and multifunctional nanocellulose aerogels for oil/water separation: a review, 2023/01/15/ Carbohydr. Polym. 300, 120242. https://doi.org/10.1016/j.carbpol.2022.120242.

Gümüşkaya, E., Usta, M., Balaban, M., 2007. Carbohydrate components and crystalline structure of organosolv hemp (Cannabis sativa L.) bast fibers pulp. Bioresour. Technol. 98 (3), 491–497.

Jiang, Y.-H., Zhang, Y.-Q., Wang, Z.-H., An, Q.-D., Xiao, Z.-Y., Xiao, L.-P., Zhai, S.-R., 2022. Cotton-derived Green sustainable membrane with tailored wettability interface: synergy of lignin and ethyl cellulose, 2022/09/01/ Ind. Crops Prod. 183, 114993. https://doi.org/10.1016/j.indcrop.2022.114993.

Jiang, Y.-H., Zhang, Y.-Q., Gao, C., An, Q.-D., Xiao, Z.-Y., Zhai, S.-R., 2022. Superhydrophobic aerogel membrane with integrated functions of biopolymers for efficient oil/water separation, 2022/02/01/ Sep. Purif. Technol. 282, 120138. https://doi.org/10.1016/j.seppur.2021.120138.

Jin, H., Zhou, X., Gu, Y., Dai, C., Yun, S., Mao, P., Guan, G., Chen, J., 2022. Multifunctional melamine formaldehyde composite foam for high-temperature insulation, flame retardancy, and oil–water separation. Ind. Eng. Chem. Res. 61 (19), 6458–6467.

Kaur, J., Sharma, K., Kaushik, A., 2023. Waste hemp-stalk derived nutrient encapsulated aerogels for slow release of fertilizers: a step towards sustainable agriculture. J. Environ. Chem. Eng. 11 (3). https://doi.org/10.1016/j.jece.2023.109582.

Kleindienst, S., Paul, J.H., Joye, S.B., 2015. Using dispersants after oil spills: impacts on the composition and activity of microbial communities, 2015/06/01 Nat. Rev. Microbiol. 13 (6), 388–396. https://doi.org/10.1038/nrmicro3452.

Li, J., Liu, Q., He, J., Zhao, Y., Mu, L., Liu, X., Zhang, Y., Sun, C.-L., Zhang, N., Qu, M., 2024. A review of superwetting aerogel-based oil-water separation materials, 2024/06/01/ Mater. Today Sustain. 26, 100741. https://doi.org/10.1016/j.mtsust.2024.100741.

Li, Z., Zhong, L., Zhang, T., Qiu, F., Yue, X., Yang, D., 2019. Sustainable, flexible, and superhydrophobic functionalized cellulose aerogel for selective and versatile Oil/Water separation, 2019/06/03 ACS Sustain. Chem. Eng. 7 (11), 9984–9994. https://doi.org/10.1021/acssuschemeng.9b01122.

Lyu, P., Xia, L., Liu, X., Hurren, C., Xu, W., Wang, X., 2023. Self-cleaning superhydrophobic aerogels from waste hemp noil for ultrafast oil absorption and highly efficient PM removal, 2023/02/01/ Sep. Purif. Technol. 306, 122503. https://doi.org/10.1016/j.seppur.2022.122503.

M, H., Gopakumar, D.A., Arumughan, V., Pottathara, Y.B., K. S, S., Pasquini, D., Bračič, M., Seantier, B., Nzihou, A., Thomas, S., Rizal, S., H. P. S, A.K., 2019. Robust superhydrophobic cellulose nanofiber aerogel for multifunctional environmental applications. Polymers 11 (3).

Motta, F.L., Stoyanov, S.R., Soares, J.B.P., 2018. Application of solidifiers for oil spill containment: a review, 2018/03/01/ Chemosphere 194, 837–846. https://doi.org/10.1016/j.chemosphere.2017.11.103.

Muehlenbachs, L., Cohen, M.A., Gerarden, T., 2013. The impact of water depth on safety and environmental performance in offshore oil and gas production. Energy Policy 55, 699–705.

Mulyadi, A., Zhang, Z., Deng, Y., 2016. Fluorine-free oil absorbents made from cellulose nanofibril aerogels. ACS Appl. Mater. Interfaces 8 (4), 2732–2740.

Paulauskiene, T., Sirtaute, E., Uebe, J., 2023. A cellulose aerogel made from paper and hemp waste added with starch for the sorption of oil. J. Mar. Sci. Eng. 11 (7). https://doi.org/10.3390/jmse11071343.

Qiao, L., Wang, M., Zhou, Z., He, Z., 2025. Non-fluorinated and photothermal lignin microspheres/candle soots-based superhydrophobic sponge for crude oil recovery and separation of oil/water mixtures and emulsions, 2025/09/05/ J. Hazard. Mater. 495, 138909. https://doi.org/10.1016/j.jhazmat.2025.138909.

Sadat Fazel, S., Jonoobi, M., Pourtahmasi, K., Sepahvand, S., Ashori, A., 2024. Enhancing the oil adsorption properties of cellulose nanofiber aerogels through chemical modification, 2024/03/01 J. Polym. Environ. 32 (3), 1304–1313. https://doi.org/10.1007/s10924-023-03037-z.

Stevulova, N., Cigasova, J., Estokova, A., Terpakova, E., Geffert, A., Kacik, F., Singovszka, E., Holub, M., 2014. Properties characterization of chemically modified hemp hurds. Materials 7 (12), 8131–8150. https://doi.org/10.3390/ma7128131.

Viscusi, G., Barra, G., Gorrasi, G., 2020. Modification of hemp fibers through alkaline attack assisted by mechanical milling: effect of processing time on the morphology of the system, 2020/10/01 Cellulose 27 (15), 8653–8665. https://doi.org/10.1007/s10570-020-03406-0.

Viscusi, G., Napolitano, F., Gorrasi, G., 2024. Modified hemp fibers as a novel and Green adsorbent for organic dye adsorption: adsorption, kinetic studies and modeling, 2024/06/01 Eur. Mediterr. J. Environ. Integr. 9 (2), 591–604. https://doi.org/10.1007/s41207-024-00463-w.

Wang, C., Lü, Y., Song, C., Zhang, D., Rong, F., He, L., 2022. Separation of emulsified crude oil from produced water by gas flotation: a review, 2022/11/01/ Sci. Total Environ. 845, 157304. https://doi.org/10.1016/j.scitotenv.2022.157304.

Wang, Q., Zhu, J., Yu, F., Li, Y., Zhang, Y., Peng, X., He, D., Zhao, S., Zheng, W., Shang, J., 2023. A thermoplastic polyurethane-based composite aerogel with low shrinkage and high specific surface area enhanced by activated carbon for highly efficient oil/water separation. J. Environ. Chem. Eng. 11 (5), 111077.

Wang, Y., Wang, M., Liu, X., Liu, T., Zhang, C., Zhao, X., Li, Z., 2024. Multifunctional aerogels with thermal insulation, elasticity, and hydrophobicity derived from hemp stems. Ind. Crops Prod. 218. https://doi.org/10.1016/j.indcrop.2024.118932.

Yu, J., Cao, C., Pan, Y., 2021. Advances of adsorption and filtration techniques in separating highly viscous crude Oil/Water mixtures. Adv. Mater. Interfaces 8 (16), 2100061. https://doi.org/10.1002/admi.202100061.

Zamparas, M., Tzivras, D., Dracopoulos, V., Ioannides, T., 2020. Application of sorbents for oil spill cleanup focusing on natural-based modified materials: a review. Molecules 25 (19), 4522.

Zhai, Y., Yuan, X., Cheng, L., Wu, H., 2023. Superhydrophobic cellulose-based aerogel derived from phormium tenax (harakeke) for efficient oil sorption, 2023/10/15/ Ind. Crops Prod. 202, 116981. https://doi.org/10.1016/j.indcrop.2023.116981.

Zhang, H., Wang, J., Xu, G., Xu, Y., Wang, F., Shen, H., 2021. Ultralight, hydrophobic, sustainable, cost-effective and floating kapok/microfibrillated cellulose aerogels as speedy and recyclable oil superabsorbents, 2021/03/15/ J. Hazard. Mater. 406, 124758. https://doi.org/10.1016/j.jhazmat.2020.124758.

Zhang, W., Liu, Y., Tao, F., An, Y., Zhong, Y., Liu, Z., Hu, Z., Zhang, X., Wang, X., 2023. An overview of biomass-based Oil/Water separation materials, 2023/07/01/ Sep. Purif. Technol. 316, 123767. https://doi.org/10.1016/j.seppur.2023.123767.

Zhou, S., Liu, P., Wang, M., Zhao, H., Yang, J., Xu, F., 2016. Sustainable, reusable, and superhydrophobic aerogels from microfibrillated cellulose for highly effective oil/water separation. ACS Sustain. Chem. Eng. 4 (12), 6409–6416.

Zhu, J., Zhu, Y., Ye, Y., Qiu, Z., Zhang, Y., Yu, Z., Sun, X., Bressler, D.C., Jiang, F., 2023. Superelastic and ultralight aerogel assembled from hemp microfibers. Adv. Funct. Mater. 33 (22), 2300893. https://doi.org/10.1002/adfm.202300893.